JOURNAL OF GEOPHYSICAL RESEARCH, VOL. 112, D10S12, doi:10.1029/2006JD007689, 2007

Inorganic chlorine and bromine in coastal New England air during summer

William C. Keene,[1] Jochen Stutz,[2] Alexander A. P. Pszenny,[3,4] John R. Maben,[1] Emily V. Fischer,[4,5] Allen M. Smith,[1,6] Roland von Glasow,[7,8] Susanne Pechtl,[7,9] Barkley C. Sive,[3] and Ruth K. Varner[3]

Received 22 June 2006; revised 26 December 2006; accepted 4 January 2007; published 8 May 2007.

[1] During summer 2004, a comprehensive suite of reactive trace gases (including halogen radicals and precursors, ozone, reactive N, soluble acids, and hydrocarbons), the chemical and physical characteristics of size-resolved aerosols, actinic flux, and related physical conditions were measured at Appledore Island, Maine, as part of the International Consortium for Atmospheric Research on Transport and Transformation (ICARTT). Sea-salt mass averaged 4 to 8 times lower than that over the open North Atlantic Ocean. Production in association with sea salt was the primary source for inorganic Cl and Br. Acid displacement of sea-salt Cl^- primarily by HNO_3 sustained high HCl mixing ratios (often >2000 pptv) during daytime. Median pHs for the larger sea-salt size fractions (geometric mean diameters, GMDs $\geq$ 2.9 μm) ranged from 3.1 to 3.4; median pHs for sub-μm size fractions were $\leq$ 1.6. Cl* (including HOCl and Cl_2) ranged from <20 to 421 pptv Cl but was less than the detection limit (DL) during most sampling intervals. Periods during which Cl* was consistently detectable corresponded to relatively clean conditions, multiday transport over water, and relatively low actinic flux. At high HCl mixing ratios (>1000 pptv), HCl + OH sustained steady state Cl-atom concentrations in the range of 10^4 cm^{-3}. When detectable, photolysis of Cl* was generally the dominant source of atomic Cl; steady state concentrations of Cl atoms were frequently in the range of 10^4 to 10^5 cm^{-3}. At these concentrations, Cl played an important role in the chemical evolution of polluted coastal air. Br radical chemistry was relatively unimportant.

Citation: Keene, W. C., J. Stutz, A. A. P. Pszenny, J. R. Maben, E. V. Fischer, A. M. Smith, R. von Glasow, S. Pechtl, B. C. Sive, and R. K. Varner (2007), Inorganic chlorine and bromine in coastal New England air during summer, *J. Geophys. Res.*, *112*, D10S12, doi:10.1029/2006JD007689.

1. Introduction

[2] Multiphase chemical transformations involving halogenated compounds impact important, interrelated chemical processes in the marine boundary layer (MBL). The emission of inorganic Cl^- and Br^- in association with sea-salt aerosol produced by wind stress at the ocean surface is the dominant source of reactive Cl and Br in marine air [*Keene et al.*, 1999; *Sander et al.*, 2003]. In most regions, rapid acidification of fresh deliquesced aerosol by HNO_3 and other acids displaces Cl^- as HCl [*Chameides and Stelson*, 1992]; the associated phase partitioning of HCl regulates aerosol pH and related pH-dependent reactions [*Keene et al.*, 1998]. In addition, particulate Cl^- and Br^- in acidic aerosol solutions are ''activated'' and subsequently recycled via autocatalytic pathways involving hypohalous acids [e.g., *Vogt et al.*, 1996]:

$$HOBr + Br^- + H^+ \rightarrow Br_2 + H_2O \quad (1)$$

$$HOCl + Br^- + H^+ \rightarrow BrCl + H_2O \quad (2)$$

$$HOCl + Cl^- + H^+ \rightarrow Cl_2 + H_2O \quad (3)$$

At night, the surface reaction

$$N_2O_5 + Cl^- \rightarrow ClNO_2 + NO_3^- \quad (4)$$

[1]Department of Environmental Sciences, University of Virginia, Charlottesville, Virginia, USA.
[2]Department of Atmospheric and Oceanic Sciences, University of California, Los Angeles, California, USA.
[3]Institute for the Study of Earth, Oceans, and Space, University of New Hampshire, Durham, New Hampshire, USA.
[4]Also at Mount Washington Observatory, North Conway, New Hampshire, USA.
[5]Now at Department of Atmospheric Sciences, University of Washington, Seattle, Washington, USA.
[6]Now at Pollard Environmental, LLC, Richmond, Virginia, USA.
[7]Institute of Environmental Physics, University of Heidelberg, Heidelberg, Germany.
[8]Now at School of Environmental Sciences, University of East Anglia, Norwich, UK.
[9]Now at Deutsches Patent- und Markenamt, Munich, Germany.

0148-0227/07/2006JD007689$09.00

may also be important [*Finlayson-Pitts et al.*, 1989]. Br_2, BrCl, Cl_2, and $ClNO_2$ volatilize and photolyze in sunlight to produce atomic Br and Cl. At high HCl concentrations (>1 ppbv) in polluted regions, significant atomic Cl is also produced via [*Singh and Kasting*, 1988]

$$HCl + OH \rightarrow Cl + H_2O. \quad (5)$$

Following production, Cl and Br atoms catalytically destroy O_3 via:

$$X + O_3 \rightarrow XO + O_2 \quad (6)$$

$$XO + HO_2 \rightarrow HOX + O_2 \quad (7)$$

$$HOX + h\nu \rightarrow OH + X \quad (8)$$

where (X = Cl and Br). Formation of halogen nitrates via XO + NO_2 and their subsequent scavenging accelerates conversion of NO_x to particulate NO_3^- and thereby contributes to net O_3 destruction [*Sander et al.*, 1999; *Pszenny et al.*, 2004]. Halogen chemistry also impacts O_3 indirectly by altering OH/HO_2 ratios (XO + HO_2 → HOX + O_2 → OH + X) [*Bloss et al.*, 2005]. These chemical pathways together with the self reaction of BrO destroy O_3 in near-surface air during Polar sunrise [*Martinez et al.*, 1999] and have also been hypothesized to explain O_3 anomalies in the MBL at lower latitudes over the western subtropical Pacific Ocean [*Nagao et al.*, 1999], the temperate Southern Ocean [*Galbally et al.*, 2000], and the tropical Indian Ocean [*Dickerson et al.*, 1999].

[3] In addition to O_3 destruction via reaction 6, atomic Cl oxidizes hydrocarbons (HCs) primarily via hydrogen abstraction to form HCl vapor and products. The enhanced supply of odd-H radicals from HC oxidation leads to O_3 production in the presence of sufficient NO_x [*Pszenny et al.*, 1993]. Evidence from the Texas Air Quality Study indicates that Cl-radical chemistry may be a significant net source for O_3 in polluted coastal/urban air [e.g., *Tanaka et al.*, 2003].

[4] Halogen-radical chemistry also provides alternate reaction pathways for S cycling in the MBL. BrO and atomic Cl efficiently oxidize $(CH_3)_2S$ [*von Glasow et al.*, 2002; *von Glasow and Crutzen*, 2004] to SO_2 in the gas phase and HOCl and HOBr oxidize S_{IV} to S_{VI} in acidic aerosol solutions [*Vogt et al.*, 1996; *Keene et al.*, 1998]. Both sets of transformations have potentially important but as yet poorly quantified influences for the nature and rate of S cycling in marine air and associated implications for aerosol production and growth, radiative transfer, and climate.

[5] Despite mounting evidence that halogen-radical chemistry is important under some tropospheric conditions, spatial and temporal variabilities in most reactant and product species, details concerning the nature of some chemical pathways, and, in polluted regions, the relative contributions and speciation of reactive halogens from anthropogenic sources remain poorly characterized. Consequently, the global significance of chemical processes involving tropospheric halogens is very uncertain. As part of the Chemistry of Halogens at the Isles of Shoals (CHAiOS) component of ICARTT, a comprehensive suite of chemical and physical characteristics of near-surface air in the northeastern U.S. coastal zone was quantified to evaluate the nature and importance of halogenated species in the chemical evolution of polluted continental outflow. In this report, we interpret the subset of observations relevant to multiphase processes involving inorganic Cl- and Br-containing species. Companion papers evaluate chemical interactions between atomic Cl and hydrocarbons [*Pszenny et al.*, 2007], iodine-radical chemistry (J. Stutz et al., Daytime OIO in the Gulf of Maine, submitted to *Geophysical Research Letters*, 2007), aerosol nucleation and growth [*Russell et al.*, 2007] and the multiphase chemical processing of HNO_3 [*Fischer et al.*, 2006] and NH_3 [*Smith et al.*, 2007]. A comprehensive modeling investigation of chlorine-radical chemistry, ozone, and related photochemical processes during ICARTT CHAiOS (S. Pechtl and R. von Glasow, Reactive chlorine in the marine boundary layer in the outflow of polluted continental air: A model study, submitted to *Geophysical Research Letter*, 2007, hereinafter reffered to as Pechtl and von Gasow, submitted manuscript, 2007) and will be published separately.

2. Methods

2.1. Sampling Site

[6] Between 6 July and 12 August 2004, ambient air was sampled on Appledore Island in the Isles of Shoals about 10 km off the southern Maine coast, USA (42.90°N, 70.62°W, Figure 1). With the exception of those noted below, inlets for sampling systems were installed on the top of a World War II-era surveillance tower about 43 m above the ocean surface. Aerosol, mist chamber, and filterpack samples were processed in a laboratory about 150 m from the tower.

2.2. Measurement Techniques

2.2.1. Reactive Trace Gases

[7] HNO_3, NH_3, HCOOH, CH_3COOH, and water-soluble, volatile inorganic Cl (hereinafter referred to as HCl) were sampled over 2-hour intervals at nominal flow rates of 20 L min^{-1} with tandem mist chambers, each of which contained 20 ml deionized water [*Keene et al.*, 2004]. All air volumes reported herein were normalized to standard temperature and pressure (0°C, 1 atm). To minimize artifact phase changes caused by mixing chemically distinct aerosol size fractions, air was sampled through a size-fractionating inlet that inertially removed super-μm aerosols from the sample stream. Sub-μm aerosol was removed downstream by an inline 47-mm Teflon filter (Zefluor 2-μm pore diameter). Samples were analyzed on site by ion chromatography (IC) usually within a few hours after recovery. Collection efficiencies for all species were greater than 95%, precisions based on paired measurements averaged ±10% to ±25%, and corresponding DLs (estimated following *Keene et al.* [1989] for both mist-chamber and aerosol samples) ranged from 3 to 11 pptv.

[8] Inorganic Cl gases were sampled in parallel with a paired set of similar tandem mist chambers samplers and an identical inlet [*Keene et al.*, 1993; *Maben et al.*, 1995; *Pszenny et al.*, 2004]. One sampler was configured with an upstream chamber containing acidic solution [37.5 mM H_2SO_4 and 0.042 mM $(NH_4)_2SO_4$] to sample HCl* (primarily HCl) and a downstream chamber containing alkaline solution [30.0 mM $NaHCO_3$ and 0.408 mM $NaHSO_3$)] to

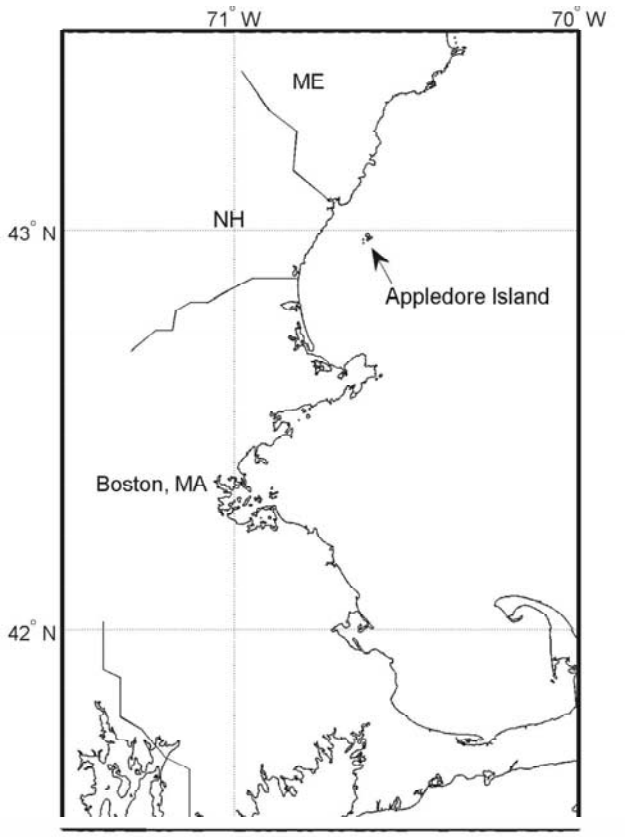

Figure 1. Location of sampling site.

sample Cl* (including Cl_2 and HOCl and presumably, ClO, Cl, $ClNO_2$, $ClNO_3$, and BrCl). The other system contained tandem chambers both of which contained alkaline solution to sample total volatile inorganic Cl (Cl_t). Available evidence [*Keene et al.*, 1993; *Maben et al.*, 1995] indicates that this sampling technique reliably discriminates volatile inorganic Cl from Cl associated with both particles and organic gases and that it quantitatively differentiates between HCl and other forms of volatile inorganic Cl. However, the speciation of Cl* cannot be determined unequivocally. Mist solutions were analyzed on site by IC. The average precision for HCl* was ±20% or ±24 pptv, whichever was the greater absolute value and that for Cl* and Cl_t was ±15% or ±10 pptv Cl, whichever was greater. Corresponding DLs were 48 pptv and 20 pptv Cl, respectively.

[9] Total volatile inorganic Br (Br_t) was sampled at a nominal rate of 85 L min^{-1} over discrete daytime (about 15-hour) and nighttime (about 9-hour) periods using a filterpack technique [*Rancher and Kritz*, 1980; *Li et al.*, 1994; *Pszenny et al.*, 2004]. An open-face, three-stage, 47-mm-diameter, polycarbonate filterpack housing was loaded with a quartz-fiber (Pallflex 2500 QAT-UP) particle filter followed by tandem rayon filters (Schleicher and Schuell, 8S) impregnated with a solution of 10% LiOH. On the basis of independent analysis of the tandem filters, collection efficiencies for the upstream filter averaged 85% for both analytes. Filterpacks were cleaned, dried, loaded, and unloaded in a class 100 clean bench. Exposed filters were transferred to polypropylene tubes, stored in glass jars, frozen, and transported to Mount Washington Observatory (MWO) for processing. Samples were spiked with 20 ng In as an internal neutron flux monitor, folded in half, and sealed in a polyethylene envelope. Samples subsequently irradiated for 5 min in a nominal neutron flux of 4×10^{12} cm^{-2} s^{-1} in the pneumatic tube facility of the Rhode Island Nuclear Science Center. Each sample was allowed to decay for approximately 5 min then counted for 900 s (live time) in fixed geometry on a high-resolution Ge(Li) gamma-ray spectrometer. Observed net counts under photopeaks at 617 keV (Br-80) and 443 keV (I-128) were corrected for decay, converted to element masses, and further corrected for neutron flux variations (based on the average In masses calculated from net counts under the 417, 819 and 1097 keV photopeaks of In-116m). The average precision for Br_t was ±19 pptv and the DL was 0.6 pptv.

[10] O_3, BrO, NO_2, and a suite of other traces gases were measured in parallel with long-path (LP) and multiaxis (MAX) differential optical absorption spectrophotometers (DOAS) [*Stutz et al.*, 2002; *Honninger et al.*, 2004]. The LP-DOAS telescope and spectrophotometer were installed in the tower approximately 8 m below the top and the retroreflector was positioned on nearby White Island, which yielded a one-way path length of 2.3 km [*Pikelnaya et al.*, 2007]. The MAX-DOAS was positioned near the base of the tower.

[11] Hourly samples were collected in 2-liter electropolished stainless steel canisters and analyzed for C_2-C_{10} nonmethane hydrocarbons (NMHCs), C_1-C_2 halocarbons, C_1-C_5 alkyl nitrates and selected sulfur compounds. Canister samples were pressurized to 35 psi using a single head metal bellows pump (MB-302MOD, Senior Flexonics, Sharon, Massachusetts) and were returned to the University of New Hampshire every 4 days for analysis by gas chromatography using two electron capture detectors (ECDs), two flame ionization detectors (FIDs) and one mass spectrometer (GC-MS) (see *Sive et al.* [2003, 2005], *Zhou et al.* [2005], and *Zhou* [2006] for additional methodological details). In addition, 60 cc aliquots were collected from the canister samples using a syringe and analyzed for methane (CH_4) by GC-FID.

2.2.2. Aerosols

[12] Ambient aerosols were sampled over discrete daytime and nighttime intervals using a modified Graseby-Anderson Model 235 cascade impactor configured with a Liu-Pui type inlet, polycarbonate substrates, and quartz-fiber backup filters (Pallflex 2500 QAT-UP) [e.g., *Pszenny et al.*, 2004]. At an average sampling rate of 1.0 m^3 min^{-1}, the average 50% aerodynamic cut diameters for the impaction stages were 18, 9.9, 3.9, 2.2, 1.1, and 0.56 μm, which yielded average GMDs for the size-resolved samples of 25, 13, 6.2, 2.9, 1.5, 0.77, and 0.39 μm. Bulk aerosol was sampled in parallel on quartz-fiber filters at an average flow rate of 1.2 m^3 min^{-1}. Impactors and bulk-filter cassettes were cleaned, dried, loaded, and unloaded in a Class 100 clean bench. Exposed substrates and filters were halved, transferred to polypropylene tubes, sealed in glass mason jars, frozen, and transported to MWO for further processing.

[13] Half sections of each substrate were extracted in 13 mL deionized water using a mini vortexer and sonica-

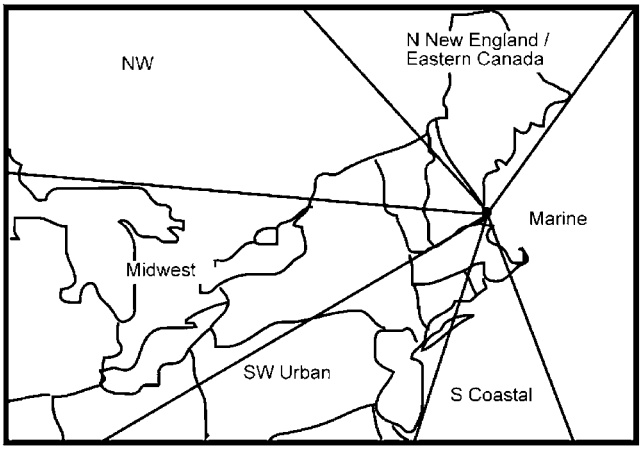

Figure 2. Major source regions for sampled air parcels.

tion; half sections of exposed backup and bulk filters were similarly extracted in 40 mL deionized water. One set of the substrate extracts and the filter extracts were analyzed by IC at MWO for total (ionized + undissociated) Cl^-, SO_4^{2-}, $CH_3SO_3^-$, $HCOO^-$, CH_3COO^-, $C_2O_4^{2-}$ NO_3^-, NH_4^+, Na^+, K^+, Mg^{2+}, and Ca^{2+} [*Keene et al.*, 2004]. Precision for total $HCOO^-$, CH_3COO^-, and Br^- averaged >±100% (i.e., most concentrations were less than DLs); precision for $CH_3SO_3^-$ and $C_2O_4^{2-}$ averaged ±15% to ±20%; precision for other analytes averaged about ±10%.

[14] The second set of substrate extracts and paired half sections of the backup and bulk filters were analyzed for total particulate Br by NAA. Five-ml aliquots of each substrate extract were spiked with 20 ng In. Two 47-mm diameter disks were punched from each backup and bulk filter, spiked with 20 ng In, folded in half, and sealed in a polyethylene envelope. Samples were subsequently analyzed using the same procedures as described above for Br_t. The average precision for particulate Br in the substrate samples was ±14% and that for the filters was ±20%. Particulate Br data reported herein correspond to those generated by NAA.

[15] Internal losses of super-μm aerosols within Sierra-type cascade impactors average about 25% to 30% [e.g., *Willeke*, 1975; *Russell et al.*, 2003]; other sources of bias for size-resolved particulate analytes based on the above procedures are generally unimportant [*Keene et al.*, 1990]. Sea-salt and non-sea-salt (nss) constituents were differentiated using Na^+ as the reference species [*Keene et al.*, 1986]. Deviations between measured and sea-salt concentrations are reported as both absolute deficits and enrichment factors (EFs) relative to sea salt [e.g., *Sander et al.*, 2003]. Because they are not conservative in bulk samples, data for total particulate and nss Cl^- (and corresponding sea-salt Cl^-) and for NO_3^- reported herein correspond to values summed over the size fractions for individual impactor samples. Data for total particulate Na^+, SO_4^{2-}, and Br correspond to bulk samples.

2.2.3. Meteorological Conditions and Atmospheric Transport

[16] Local air temperature, relative humidity (RH), and barometric pressure were measured on White Island at the Isles of Shoals, NH, meteorological station (IOSN3) operated by National Oceanic and Atmospheric Administration (NOAA). Sea surface temperature was measured at two moored buoys (44013 and 44007) operated by NOAA's National Data Buoy Center 87 km S and 80 km NE, respectively, of the sampling site.

[17] Actinic flux was quantified using a spectroradiometer (Bentham/Gigahertz Optics) deployed near the tower on Appledore Island. Postexperiment calibration revealed negative bias in these measurements. During midday, the approximate error was 7.5% under clear-sky conditions and up to 50% under cloudy conditions. Consequently, the corresponding calculated values reported herein (including photolysis rates, OH concentrations, and Cl-atom production rates and concentrations, see next section) are considered lower limits.

[18] Large-scale atmospheric transport was evaluated using both HYbrid Single-Particle Lagrangian Integrated Trajectories (HYSPLIT) [*Draxler and Rolph*, 2005] provided by the Plymouth State Weather Center and Lagrangian particle dispersion (FLEXPART) retroplumes [*Stohl et al.*, 2005]. Samples were classified by source region (Figure 2) on the basis of visual inspection of the back trajectories and the corresponding column and footprint residence time components of the retroplumes [*Fischer et al.*, 2006].

2.3. Calculations

2.3.1. Aerosol pH, OH, and Atomic Cl

[19] Aerosol pH was inferred on the basis of the measured phase partitioning and associated thermodynamic properties (Henry's Law and dissociation constants) of HCl, meteorological conditions (RH and temperature), and hygroscopicity models of aerosol liquid water content (LWC) [*Keene et al.*, 2004]. OH concentrations were calculated on the basis of the measured O_3, NO_2, actinic flux, and associated photolysis rates following the parameterization of *Ehhalt and Rohrer* [2000]. The sources and sinks for atomic Cl that were evaluated in this analysis are summarized in Table 1. While not comprehensive, this suite of reactions includes the major production and destruction pathways that are likely to be important in controlling Cl-atom concentrations in coastal New England during summer. Concentrations of hydrocarbons measured during the campaign are reported in companion papers [*Pszenny et al.*, 2007; J. L. Ambrose et al., Nighttime nitrate radical chemistry at Appledore Island, ME during ICARTT 2004, submitted to *Journal of Geophysical Research*, 2007]. Photolysis rates (J values) for Cl gases were calculated from the cited cross sections and the measured actinic fluxes (Table 1 and Figure 3h). Steady state Cl-atom concentrations were calculated as follows:

$$[Cl] = \left(k_1^*[HCl]^*[OH] + J_i^*\left[Cl^*\right]\right) / \left(k_2^*[O_3] + \Sigma k_j^*\left[HC_j\right]\right) \quad (9)$$

where all concentrations units are in molecules cm^{-3}; k is the rate constant corresponding to each indicated reaction (Table 1); HCl (Figure 3e), Cl* (Figure 3f), and O_3 were measured; and OH was calculated (Figure 3h). HC_j refers to the subset of measured hydrocarbons with which reaction is an important sink for atomic Cl. These include CH_4, ethane (C_2H_6), ethene (C_2H_4), ethyne (C_2H_2), propane (C_3H_8), propene (C_3H_6), n-butane (n-C_4H_{10}), i-butane (i-C_4H_{10}), n-pentane (n-C_5H_{12}), i-pentane (i-C_5H_{12}), isoprene (C_5H_8), α-pinene (α-$C_{10}H_{16}$), β-pinene (β-$C_{10}H_{16}$), and camphene

Table 1. Sources and Sinks for Atomic Cl Evaluated in This Analysis

Reaction	Rate Constant (298 K, 1 atm)	Reference
Sources		
$HCl + OH \rightarrow Cl + H_2O$	8×10^{-13} molecules cm^{-3} s^{-1}	*DeMore et al.* [1997]
$Cl_2 + hv \rightarrow 2\ Cl$	$J(Cl_2)$, s^{-1} (Figure 3h)	*DeMore et al.* [1997]
$HOCl + hv \rightarrow Cl + OH$	J(HOCl), s^{-1} (Figure 3h)	*DeMore et al.* [1997]
$ClNO_2 + hv \rightarrow Cl + NO_2$	$J(ClNO_2)$, s^{-1} (Figure 3h)	*DeMore et al.* [1997]
$ClNO_3 + hv \rightarrow Cl + NO_3$	$J(ClNO_3)$, s^{-1}[a]	*DeMore et al.* [1997]
Sinks		
$Cl + O_3 \rightarrow ClO + O_2$	1.2×10^{-11} molecules cm^{-3} s^{-1}	*DeMore et al.* [1997]
$Cl + CH_4 + O_2 \rightarrow HCl + CH_3OO$	1.0×10^{-13} molecules cm^{-3} s^{-1}	*Atkinson et al.* [2005]
$Cl + C_2H_6 \rightarrow HCl + C_2H_5$	5.9×10^{-11} molecules cm^{-3} s^{-1}	*Atkinson et al.* [2005]
$Cl + C_2H_4 + M \rightarrow C_2H_4Cl + M$	3×10^{-10} molecules cm^{-3} s^{-1}	*Atkinson et al.* [2005]
$Cl + C_2H_2 + M \rightarrow C_2H_2Cl + M$	2.0×10^{-10} molecules cm^{-3} s^{-1}	*Atkinson et al.* [2005]
$Cl + C_3H_8 \rightarrow HCl + C_3H_7$	1.40×10^{-10} molecules cm^{-3} s^{-1}	*Atkinson et al.* [2005]
$Cl + C_3H_6 + M \rightarrow C_3H_6Cl + M$	2.8×10^{-10} molecules cm^{-3} s^{-1}	*Atkinson et al.* [2005]
$Cl + n\text{-}C_4H_{10} \rightarrow HCl + C_4H_9$	2.05×10^{-10} molecules cm^{-3} s^{-1}	*Atkinson et al.* [2005]
$Cl + i\text{-}C_4H_{10} \rightarrow HCl + C_4H_9$	1.43×10^{-10} molecules cm^{-3} s^{-1}	*Atkinson* [1997]
$Cl + n\text{-}C_5H_{12} \rightarrow HCl + C_5H_{11}$	2.80×10^{-10} molecules cm^{-3} s^{-1}	*Atkinson* [1997]
$Cl + i\text{-}C_5H_{12} \rightarrow HCl + C_5H_{11}$	2.20×10^{-10} molecules cm^{-3} s^{-1}	*Atkinson* [1997]
$Cl + C_5H_8 \rightarrow$ products	5.1×10^{-10} molecules cm^{-3} s^{-1}	*Finlayson-Pitts et al.* [1999]
$Cl + \alpha\text{-}C_{10}H_{16} \rightarrow$ products	4.6×10^{-10} molecules cm^{-3} s^{-1}	*Finlayson-Pitts et al.* [1999]
$Cl + \beta\text{-}C_{10}H_{16} \rightarrow$ products	5.3×10^{-10} molecules cm^{-3} s^{-1}	*Finlayson-Pitts et al.* [1999]
$Cl + C_{10}H_{16} \rightarrow$ products	6.2×10^{-10} molecules cm^{-3} s^{-1}[b]	*Finlayson-Pitts et al.* [1999]

[a]For a given actinic flux, the photolysis rate of $ClNO_3$ is about an order of magnitude lower than that of HOCl; to minimize congestion of Figure 3h, $J(ClNO_3)$ values are not depicted.

[b]Estimated on the basis of the average of rate constants for other nonpinene $C_{10}H_{16}$ biogenic hydrocarbons including limonene, myrcene, and 3-carene (6.4, 6.6, and 5.6×10^{-10} molecules cm^{-3} s^{-1}, respectively).

($C_{10}H_{16}$). As described in more detail below, the sensitivity of Cl-atom production was evaluated over a range of assumed Cl* speciation on the basis of the corresponding J values for each (J_i).

2.3.2. Dry-Deposition Fluxes

[20] Dry-deposition fluxes of size-resolved particulate phase species to the coastal ocean were modeled on the basis of the measured chemical composition and GMD for each size fraction, wind velocity, air temperature, and RH following *Hummelshøj et al.* [1992]. The laminar sublayer was assumed to be at 98% RH [*Lewis and Schwartz*, 2004]; the corresponding GMD for each size fraction in the sublayer was based on the measured ionic composition and hygroscopicity models (the same as those used to estimate aerosol LWC in the overlying air; see above). Dry-deposition fluxes of HCl to the surface ocean were calculated on the basis of the measured mixing ratios, wind speed, air temperature, and surface-ocean-water temperature following *Valigura* [1995]. The latter approach assumes that the surface ocean is substantially undersaturated with respect to gaseous inorganic Cl and Br species and, thus, solubility does not limit corresponding dry-deposition fluxes. We also assume no vertical gradients in particulate and gas phase species between the reference height for the approaches (10 m) and the measurement height (43 m).

3. Results and Discussion

3.1. Volatile Inorganic and Particulate Cl and Br Species in Ambient Air

[21] Concentrations of particulate and vapor phase species measured during this campaign (Figure 3 and Table 2) covered broad dynamic ranges that were similar to those quantified in the same region during summer 2002 [e.g., *Keene et al.*, 2004]. Relative size distributions of Na^+ were similar to those over the open ocean with maximum concentrations associate with super-μm size fractions (Figure 4a). However, the average Na^+ concentration during the campaign (Table 2) was 4.5 times less than the annual average over the western Atlantic Ocean at Bermuda and 6 to 7 times less than those over the southeastern North Atlantic at Barbados and the northwestern North Atlantic at Mace Head Ireland [*Galloway et al.*, 1993]. Relative to the composition of fresh sea-salt aerosol, most samples were significantly depleted in Cl^- (Figures 3d and 3e). On the basis of median values, the GMD 1.52- and 0.77-μm size fractions exhibited the greatest relative depletions (Figure 4d). The median Cl^- EF for all size-resolved samples was 0.66. Cl^- EFs based on size-resolved samples from less polluted and remote marine regions generally range from 0.80 to 0.95 [e.g., *Graedel and Keene*, 1995; *Pszenny et al.*, 2004].

[22] A reduced major axis (RMA) regression of all detectable paired HCl* and HCl data (N = 253) yielded a slope of 1.03, an intercept of −35 pptv and a correlation coefficient of 0.98; the slope and intercept were statistically indistinguishable from 1 and 0, respectively. The good agreement between these paired data reflects the fact that HCl was the dominant form of volatile inorganic Cl during the campaign (discussed in more detail below). Because HCl sampled with the dionized-water mist chambers exhibited relatively greater precision and a lower DL, associated interpretations reported herein are based primarily on those data.

[23] HCl mixing ratios ranged from 5 to 5727 pptv and generally peaked during daytime (Figure 3e). The average and median HCl mixing ratios (Table 2) fell within the range of values measured under moderately polluted conditions at Bermuda during spring (12-hour averages from 133 to 883 pptv [*Keene and Savoie*, 1998]) but were greater

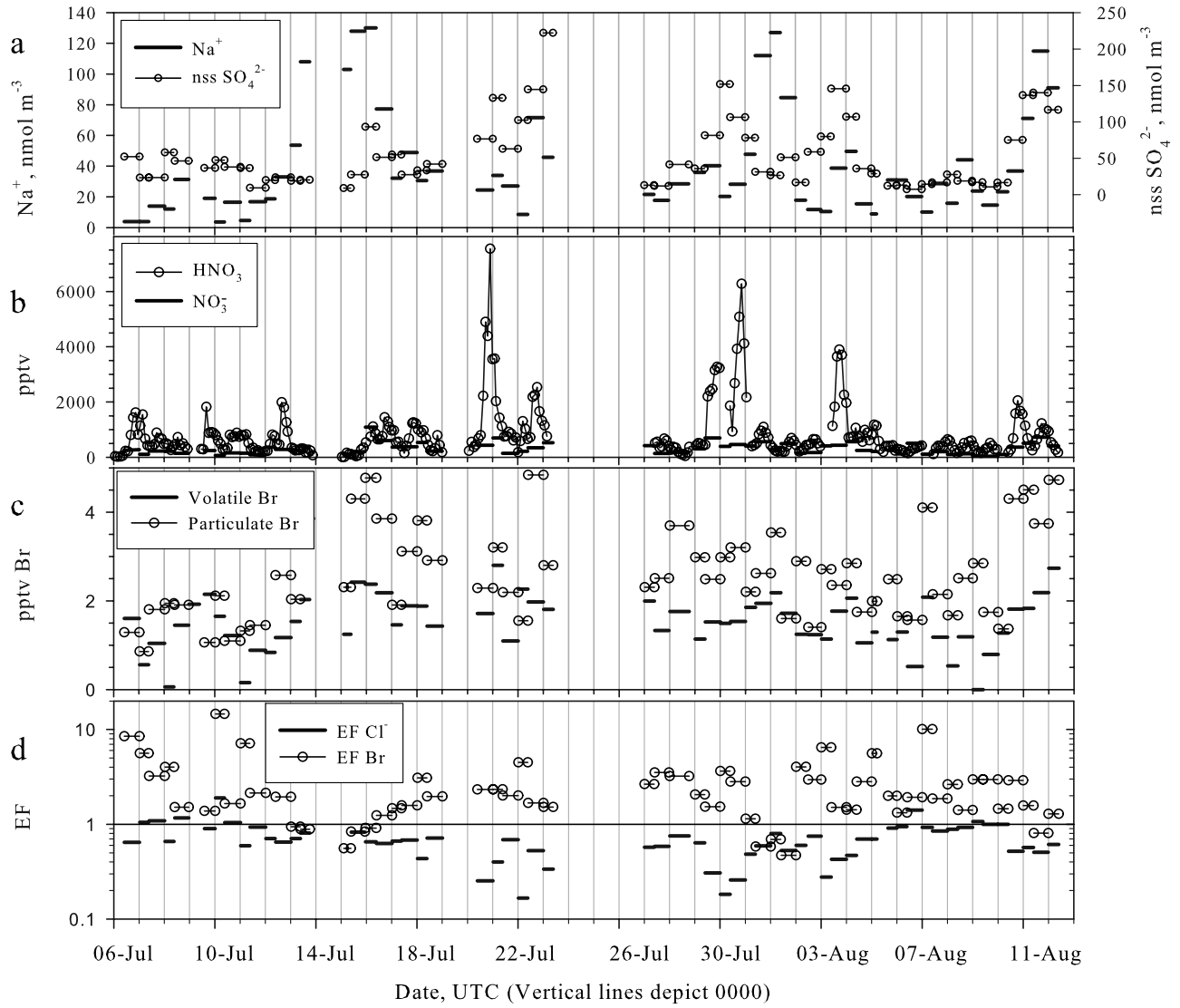

Figure 3. Time series of (a) particulate Na^+ and nss SO_4^{2-}; (b) HNO_3 and particulate NO_3^-; (c) volatile inorganic and particulate Br; (d) EFs for particulate Cl^- and Br; (e) HCl and particulate Cl^- deficit; (f) Cl*; (g) calculated OH; (h) J_{Cl2}, J_{HOCl}, and J_{ClNO2}; (i) calculated production rate of atomic Cl from HCl + OH and from HCl + OH plus Cl* photolysis based on the assumption that Cl* is in the form of Cl_2 or HOCl; and (j) corresponding calculated steady state concentration of atomic Cl based on the three production scenarios depicted in Figure 3i. Values less than the DL are plotted as 0.5 times the DL. To facilitate direct comparison with the vapor phase, particulate species in Figure 3b (NO_3^-), Figure 3c (Br), and Figure 3e (Cl^- deficit) are plotted in units of pptv equivalents.

than those measured at Hawaii during late summer (27 to 263 pptv [*Pszenny et al.*, 2004]).

[24] To characterize relative diel variability over the course of the experiment, HCl mixing ratios measured during each individual day (based on the midpoint of the sampling interval) were scaled from 0 to 1 by subtracting the minimum for the day and then dividing by the range for that day. The ranked values for all days were then binned into twelve 2-hour increments (e.g., 2300 to 0100; 0100 to 0300, etc.) and plotted (Figure 5). On the basis of median values, HCl increased rapidly following sunrise, peaked around local noon, decreased during the afternoon, exhibited a minor secondary peak following sunset, and decreased to minimum values near dawn. The diel variability of HNO_3 exhibited a similar pattern [*Fischer et al.*, 2006]. Photochemical production during the day (discussed in more detail below) contributed to the midday peak. However, the depth of the mixed layer over the upwind continent also varied over diel cycles in response to surface heating [*Arya*, 2001] and thereby contributed to variability in the composition of near-surface air sampled at Appledore. At night, HCl in the relatively shallow, coastal mixed layer was depleted via dry deposition to the surface and scavenging by fresh (unsaturated) sea-salt aerosol. As the depth of the mixed layer increased over land in response to heating following sunrise, air from aloft that was not

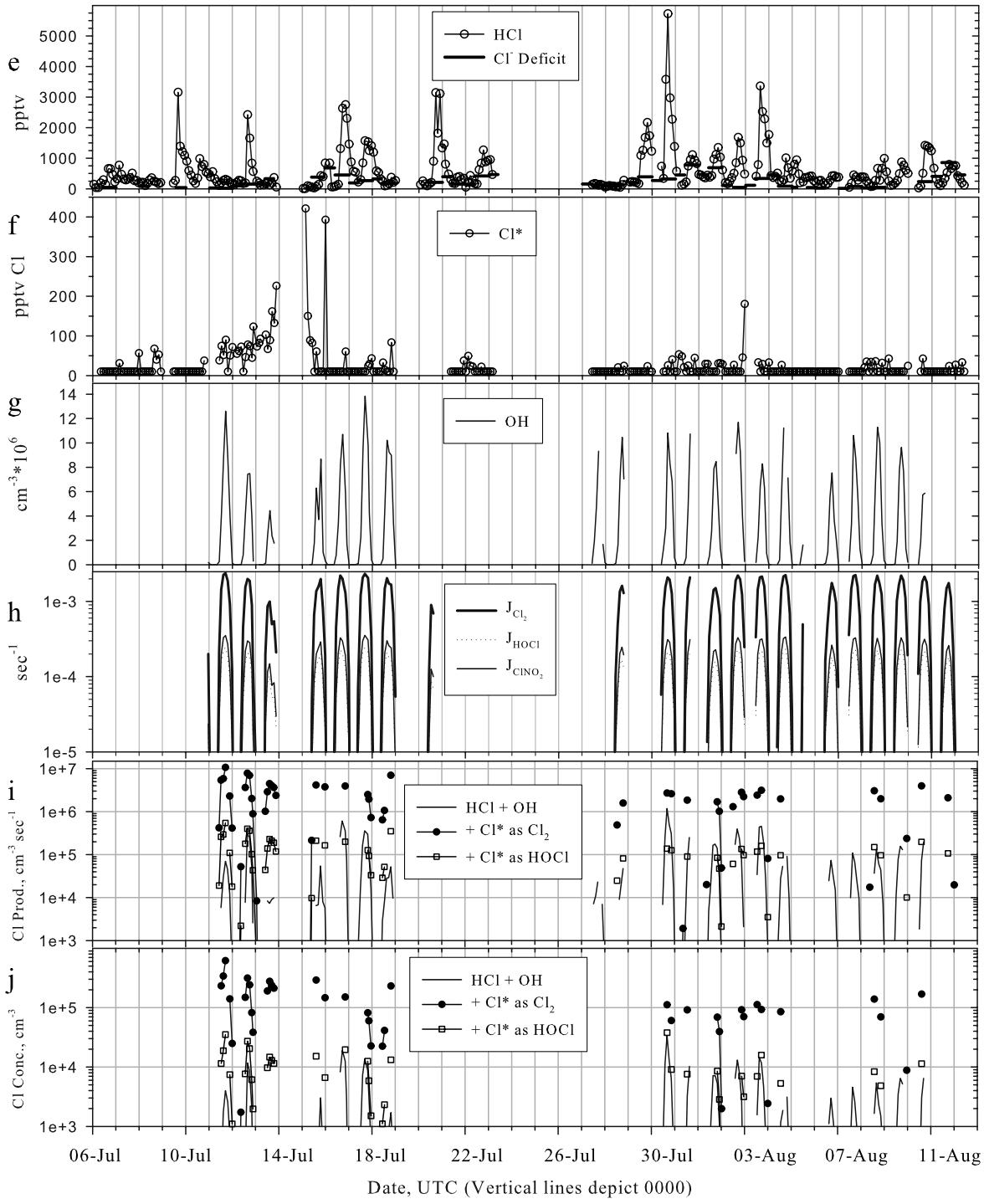

Figure 3. (continued)

Table 2. Summary Statistics

Statistic	Particulate Na^+, nmol m^{-3}	Particulate Cl^-, nmol m^{-3}	Particulate Br, nmol m^{-3}	HCl, pptv	Cl*, pptv	Volatile Br, pptv
Maximum	130	82.8	0.216	5728	421	2.80
75th percentile	48.1	20.9	0.142	774	25	1.93
Median	29.6	14.1	0.111	351	<20	1.53
25th percentile	16.7	7.9	0.079	193	<20	1.17
Minimum	3.6	1.2	0.038	5	<20	<0.06
Average[a]	40.2	19.4	0.115	599	10	1.50
Number	60	60	59	302	272	61

[a]Values below DLs are included in averages.

depleted by nocturnal deposition and scavenging of either HCl or HNO_3 [*Fischer et al.*, 2006] (which reacts with sea salt to produce HCl, see below) was entrained into the mixed layer thereby contributing to rising concentrations in near-surface air during morning.

[25] Although most Cl* mixing ratios during this experiment were below the DL, the maximum value reached 421 pptv Cl. (Table 2 and Figure 3f). The lack of an obvious diel cycle during periods when Cl* was detectable is consistent with modeled diel variabilities in major components of Cl* (HOCl, Cl_2, ClO, BrCl, and Cl) at Hawaii [*Pszenny et al.*, 2004]. Under those cleaner conditions, Cl_2 and BrCl peak at night whereas the other species peak during the day but at different times and, consequently, Cl* exhibits relatively little diel variability. The range in Cl* at Appledore was similar to that reported by *Pszenny et al.* [1993] (<26 to 254 pptv Cl) for coastal southern Florida during January. In contrast, the range in Cl* under cleaner conditions at Hawaii during late summer was substantially lower (<3 to 38 pptv Cl [*Pszenny et al.*, 2004]). Assuming that Cl_2 was a significant component of Cl* at night [*Pszenny et al.*, 2004], the range in measured Cl* during this campaign is consistent with the range of Cl_2 measured at night on the Long Island, New York, coast (<10 to 150 pptv [*Spicer et al.*, 1998]) but somewhat greater than that for more recent measurements in coastal urban air in southern California (<5 to 40 pptv [*Finley and Saltzman*, 2006]). Note that in the above summary, Cl_2 is reported as pptv Cl_2 whereas Cl* is reported as pptv Cl.

[26] Between 1848 on 10 July and 0532 on 15 July, Cl* was detected during most sampling intervals and 7 of the 9 mixing ratios greater than 100 pptv Cl that were measured during the campaign occurred during this period (Figure 3f). The period also coincided with relatively strong surface winds with a marine fetch as reflected in high sea-salt concentrations (Figure 3a), relatively low levels of pollutant species (e.g., HNO_3 and nss SO_4^{2-}, Figures 3a and 3b), and relatively low actinic flux (e.g., as indicated by calculated OH and J values, Figures 3g and 3h, respectively). Sampling was suspended for most of 14 July because of precipitation. From early on 13 July through early on 15 July when the highest persistent mixing ratios were measured, trajectories and retroplumes indicate large-scale atmospheric transport from the marine sectors (marine and southwest coastal, Figure 2) with residence times in the MBL greater than 1 day. Throughout the period, temperatures were cool, the sky was overcast, and mist was frequent. We hypothesize that the relatively low photolytic sink for volatile inorganic Cl (Figure 3h) contributed to the accumulation of Cl* to higher concentrations during this relative to other periods. In addition, the relatively high concentrations of sea-salt aerosol (including precursor Cl^-) during the period (Figure 3a) may have also sustained higher production rates of Cl*. We return to this point below.

[27] The high Cl* and low HCl (and corresponding Cl_t and HCl*) mixing ratios during this relative to other sampling periods (Figures 3e and 3f) correspond to conditions under which the overall reliability of these data can be independently evaluated. Because total volatile inorganic Cl (Cl_t) is approximately equal to sum of HCl* and Cl*, differences between Cl_t and HCl* (ΔCl) are approximately equal to the corresponding Cl* mixing ratios [*Maben et al.*, 1995]. Consequently, a regression of these values should have a slope of approximately 1.0 and an intercept of approximately 0.0. A reduced major axis regression of ΔCl versus Cl* for all corresponding sampling intervals during which Cl_t, HCl*, and Cl* were detectable (N = 20 excluding one outlier) yielded a significant linear relationship with a slope of 0.79, a Y intercept of 19 pptv, and a correlation coefficient of 0.63; the slope and intercept were statistically indistinguishable from 1 and 0, respectively. Because ΔCl typically corresponded to small differences between substantially larger and uncertain values (see section 2), accumulated measurement uncertainties contribute to overall uncertainty in this comparison. However, the reasonable agreement between the paired values provides independent corroboration that significant Cl* was present under these conditions.

[28] Concentrations of both volatile-inorganic and particulate Br (Figure 3c and Table 2) were near the lower limits of reported values over the open ocean [*Sander et al.*, 2003]. In addition, BrO was undetectable (less than about 2 pptv) by long-path and MAX DOAS throughout the campaign. Given the high pollutant loadings in coastal New England air during summer, these results are consistent with the hypothesis that inorganic bromine in the MBL originates primarily from sea salt and not anthropogenic sources. Size distributions of particulate Br relative to Na^+ reflect characteristic EFs for polluted marine air (Figure 4). On the basis of median values, the larger super-μm GMD size fractions exhibit modest depletions (EFs < 1), the smaller super-μm GMD size fractions are substantially depleted (EFs $\ll$ 1), and the sub-μm GMD size fractions are substantially enriched (EFs $\gg$ 1). When summed over all

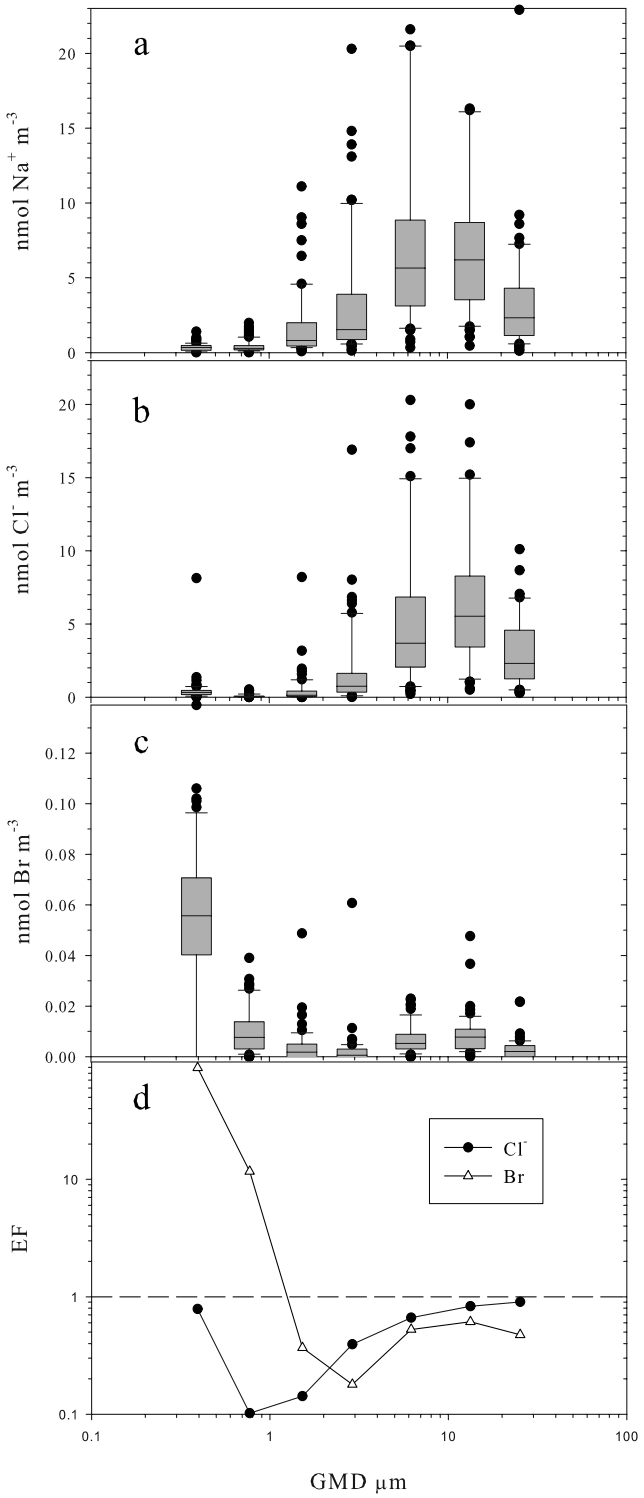

Figure 4. Size distributions of particulate (a) Na^+, (b) Cl^-, and (c) Br and d) corresponding size distributions of median EFs for Cl^- and Br. Here and elsewhere, boxes depict 25th, 50th, and 75th percentiles; whiskers depict 10th and 90th percentiles. Extreme values are plotted individually.

size fractions, most samples exhibited EFs > 1 (Figure 3d); the median EF for all samples was 1.9. EFs less than 1 were limited to the periods with relatively high sea-salt concentrations (Figure 3d). The processes responsible for accumulation of Br in sub-μm size aerosol size fractions in the presence of O_3 are not understood (see *Sander et al.* [2003] for detailed discussion). Model simulations of the halogen activation mechanism suggest that efficient recycling through acidic S aerosols should enhance production of Br_2 and BrCl relative to that expected based exclusively on reactions involving sea-salt solutions; sub-μm Br does not accumulate in the model [*Vogt et al.*, 1996]. The observed enrichments suggest several possibilities: (1) Sub-μm Br may exist in a form other than Br^-, (2) sub-μm Br may be associated with chemically distinct particles that lack sufficient water or acidity to sustain Br activation, (3) relatively thicker organic coatings on smaller size fractions may limit Br volatilization, or (4) as yet unidentified chemical pathways lead to Br accumulation in sub-μm size fractions.

3.2. Sea-Salt and Non-Sea-Salt Sources for Cl and Br Species

[29] Although production of sea-salt aerosol as a function of wind velocity is the dominant source for inorganic Cl and Br in the open ocean MBL, the transport of crustal dust and anthropogenic emissions (fossil fuel and biomass combustion, incineration, industrial processes, and chlorinated water supplies) from continents and biogenic emissions of photolytic Br-atom precursors may contribute to ambient concentrations in coastal marine air [*Keene et al.*, 1999, 2006; *Sander et al.*, 2003; *Tanaka et al.*, 2003]. During this study, the sea-salt tracers Na^+ and Mg^{2+} in most samples were present at ratios (median molar ratio = 8.42) near those of surface seawater (molar ratio = 8.82 [*Wilson*, 1975]). Ratios of Na^+ and Mg^{2+} in crustal dust (e.g., 3.14 in high-dust events at Barbados [*Arimoto et al.*, 1995]) diverge substantially from those in sea salt and noncrustal anthropogenic sources for these particulate species are generally small to negligible [*Keene et al.*, 1986]. The good agreement between the measured and sea-salt ratios of Na^+ to Mg^{2+} implies that over the coastal Gulf of Maine during summer both species and the associated sea-salt constituents originated primarily from the surface ocean. Variability in concentrations of sea-salt Cl^- and sea-salt Br^- as a function of source region (Figure 6) are driven in part by corresponding variability in wind velocities (media of 4.4, 4.3, 4.5, 8.8, and 5.4 m s^{-1} for the north, northwest, midwest, southwest, and south transport sectors, respectively) and fetch over water. Effects of more localized land-sea breeze circulation patterns and scavenging via precipitation also contribute to variability in sea-salt Cl^- and sea-salt Br^- among transport sectors. Because aerosol sampling was suspended during the frequent periods of precipitation associated with easterly flow, no paired data are available for the marine sector.

[30] Measured concentrations of particulate Cl^- were depleted relative to sea-salt Cl^- (EFs < 1) during most individual sampling intervals (Figure 3d) and, on the basis of median values, measured Cl^- was also depleted relative to sea salt for all transport regimes (Figure 6a). The greatest absolute and relative depletions were associated with transport from the more heavily populated and industrialized

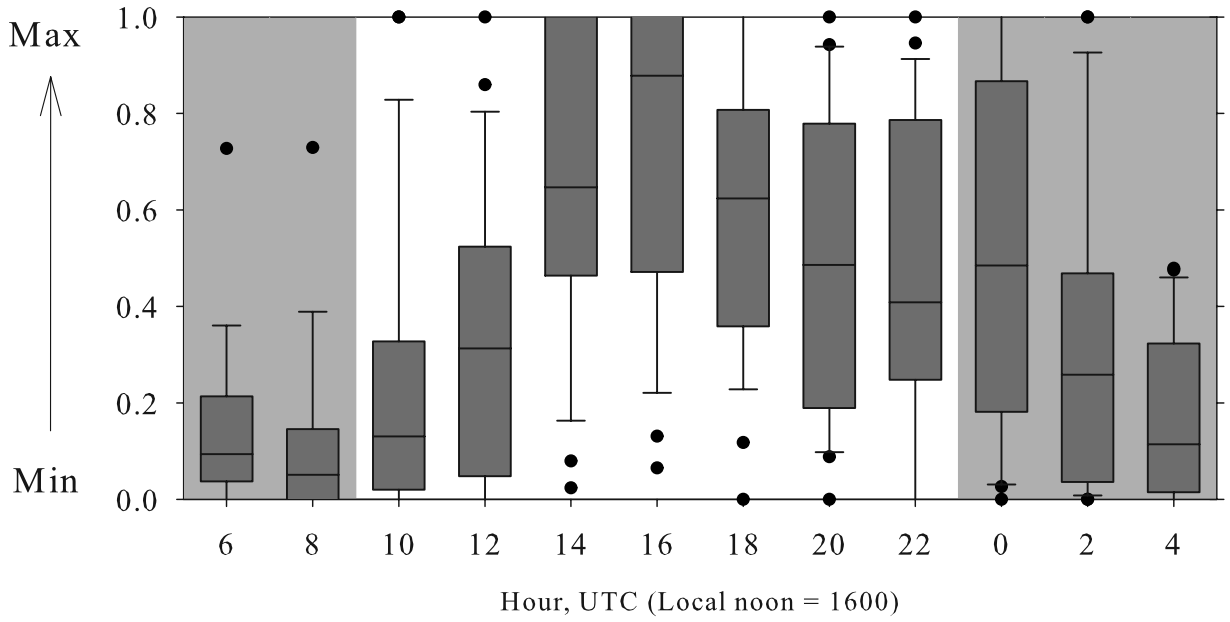

Figure 5. Normalized diel variability in HCl. The shaded area depicts night.

regions (southwest and midwest sectors). These source regions were also associated with the highest concentrations of HNO_3 [*Fischer et al.*, 2006] and nss SO_4^{2-} [*Smith et al.*, 2007] observed during the campaign as well as the highest median HCl concentrations. As discussed in more detail below, these relationships are consistent with expectations based on the pH dependence of HCl phase partitioning [*Keene et al.*, 1998; *Erickson et al.*, 1999]. During most sampling periods (Figure 3e), HCl mixing ratios were greater than the corresponding particulate Cl^- deficits relative to sea salt (Figure 3e), which implies that HCl had longer atmospheric lifetimes against deposition relative to the parent sea-salt aerosol and/or that significant HCl originated from non-sea-salt sources. We return to this point below.

[31] In contrast to particulate Cl^-, measured concentrations of particulate Br were typically enriched relative to sea-salt Br (Figure 3d). On the basis of median values for the different transport sectors, only the southwest, which was associated with the highest sea-salt concentrations, was slightly depleted (Figure 6b). In addition, unlike the situation for Cl^-, the absolute and relative magnitudes of Br enrichments did not vary systematically as a function of the more polluted (southwest and midwest) versus less polluted (north, northwest, and S coastal) transport regimes. These relationships suggest that the processes controlling Br phase partitioning were relatively insensitive to variability in levels of pollutants during this experiment. Finally, for all transport sectors, the median concentrations of particulate Br consistently exceeded those of volatile Br and the median concentrations of particulate plus volatile Br were substantially greater than corresponding sea-salt Br^- (Figure 6b). These differences suggest possible contributions of nss Br from anthropogenic or marine biogenic sources. Alternatively, the volatilization of Br from the short-lived super-μm size fractions and its subsequent accumulation in the long-lived sub-μm size fractions (Figure 4)

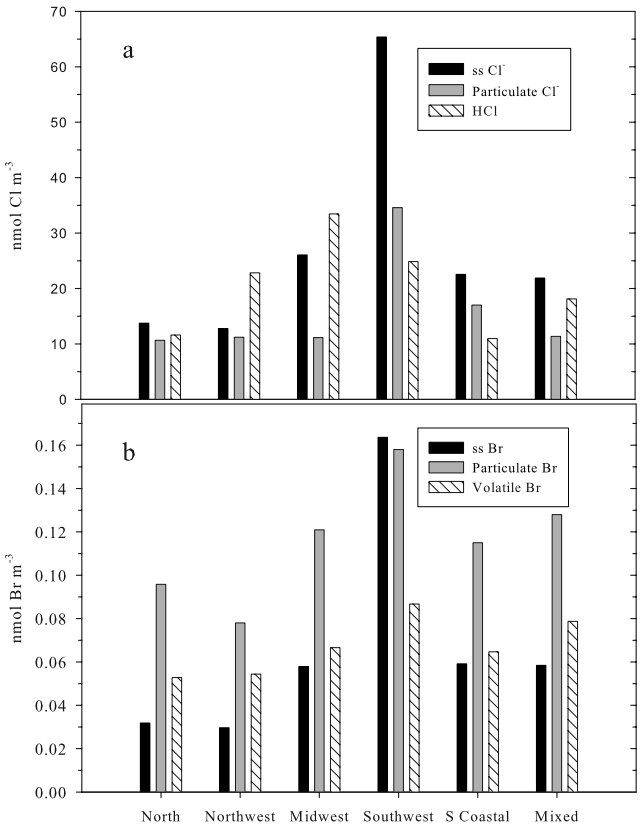

Figure 6. Median concentrations of (a) sea-salt Cl^-, measured particulate Cl^-, and HCl and (b) sea-salt Br, measured particulate Br, and volatile inorganic Br for each source region. Numbers of paired particulate and vapor phase data for the north, northwest, midwest, southwest, south coastal, and mixed sectors were 10, 15, 5, 9, 5, and 16, respectively.

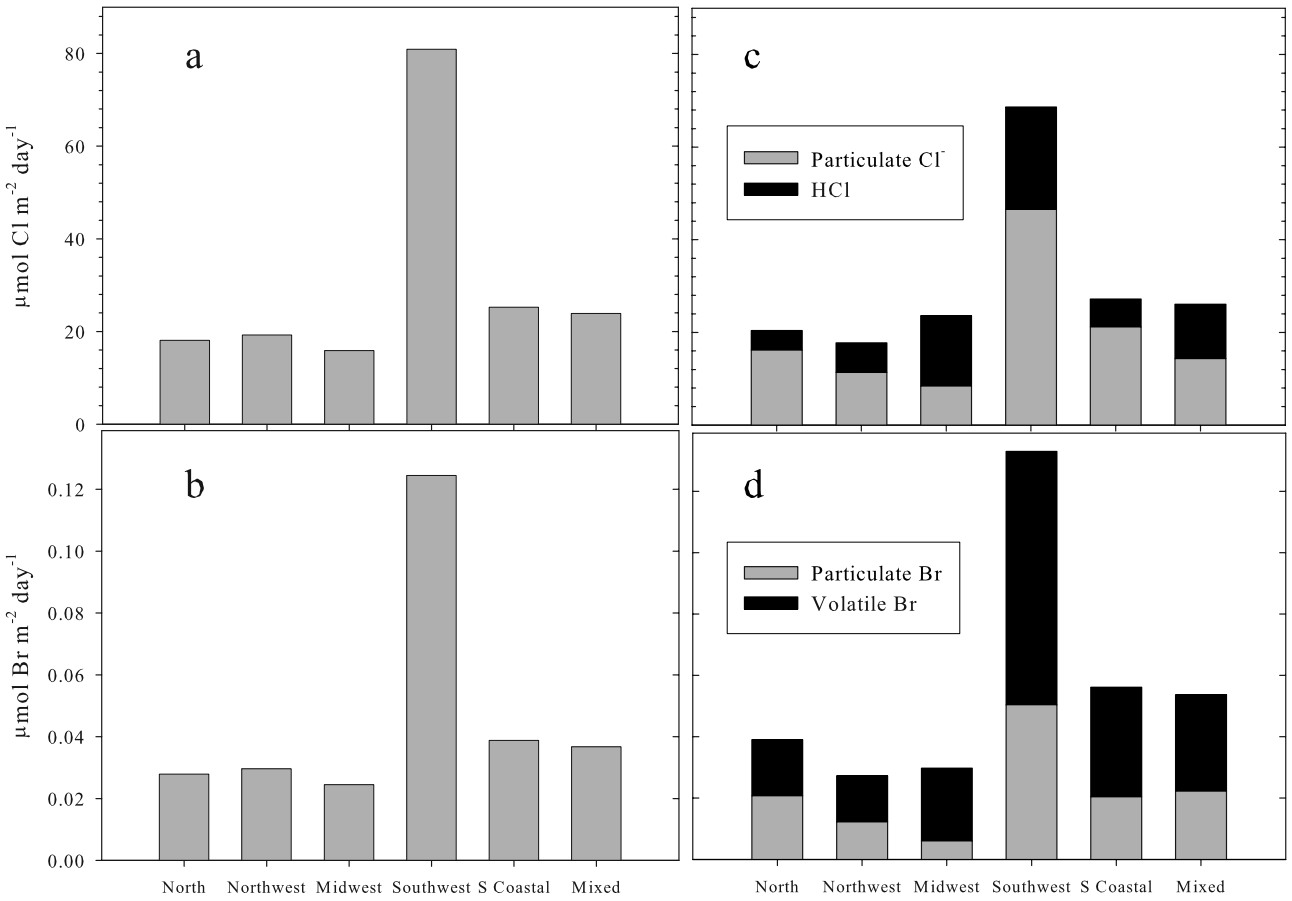

Figure 7. Median emission fluxes of (a) sea-salt Cl^- and (b) sea-salt Br inferred from modeled dry-deposition fluxes of particulate Na^+ compared with median modeled deposition fluxes of (c) HCl and particulate Cl^- and (d) volatile inorganic and particulate Br for each source region.

may have contributed to the divergence between sea-salt and total measured (particulate + volatile) Br concentrations.

[32] Under steady state conditions in the absence of precipitation, the emission flux of a conservative sea-salt tracer such as Na^+ is balanced by (and, consequently, can be estimated from) its corresponding dry-deposition flux. Similarly, at steady state, the emission fluxes of Cl^- and Br^- in association with sea-salt aerosol can be estimated on the basis of their respective ratios with a conservative sea-salt tracer such as Na^+ in seawater and the corresponding dry-deposition flux of that tracer to the ocean surface. For example, at steady state, the emission flux of sea-salt Cl^- from the surface ocean is equal to the corresponding deposition flux of particulate Na^+ multiplied by the Cl^-/Na^+ ratio in seawater. We recognize that the assumption of steady state in a dynamic coastal regime is problematic. However, on the basis of representative sample statistics for central tendencies (e.g., median values), comparisons between the inferred emission fluxes of sea-salt Cl^- and Br^- and the corresponding dry-deposition fluxes of measured volatile and particulate Cl and Br species provide a semiquantitative approach with which to evaluate the relative importance of sea-salt versus nss sources for Cl and Br during this campaign.

[33] The median emission fluxes of sea-salt Cl^- and sea-salt Br^- inferred from the dry-deposition fluxes of size-resolved Na^+ associated with each source region are compared with the corresponding deposition fluxes of total Cl (HCl + size-resolved particulate Cl^-) and total Br (volatile + size-resolved particulate Br), respectively, in Figure 7. Concentrations of Cl* were generally small to negligible relative to HCl and particulate Cl^- (Table 2 and Figures 3e and 3f) and median values for all sectors were below the DL. Consequently, Cl* was not considered in this analysis. The generally good agreement between the inferred median emission fluxes and the corresponding modeled dry-deposition fluxes for all transport regimes supports the hypothesis that sea-salt aerosol was the primary source of inorganic Cl and volatile inorganic and particulate Br in coastal New England during summer. These results suggest that divergence among sea-salt, particulate, and volatile concentrations was driven primarily by atmospheric processing rather than contributions from anthropogenic, marine biogenic, and crustal sources.

3.3. Sea-Salt Dehalogenation and Aerosol pH

[34] In addition to the similarities in their diel cycles (mentioned above), longer-term temporal variabilities of HCl and HNO_3 over the course of the experiment were

also correlated. For example, the three most polluted episodes on 20 July, 30 July, and 3 August episodes (as indicated by HNO_3 concentrations greater than 4000 pptv) coincided with three of the 4 days during which HCl mixing ratios exceeded 3000 pptv (Figure 3). The covariability of these compounds is explained in part by coupled, pH-dependent, chemical interactions with sea-salt aerosol [e.g., *Keene and Savoie*, 1998]. On the basis of its thermodynamic properties, HNO_3 partitions preferentially with relatively less acidic (compared to sub-μm S aerosols) sea-salt size fractions according the following relationship:

$$HNO_{3g} = \left(\left\{NO_3^-\right\} * H^+\right) / \left(K_{H\text{-}HNO3} * K_{a\text{-}HNO3}\right) \quad (10)$$

where activities are in M, $K_{H\text{-}HNO3}$ is the Henry's Law constant for HNO_3 in M atm^{-1}, and $K_{a\text{-}HNO3}$ is the acid dissociation constant for HNO_3 in M. The resulting acidification of sea-salt aerosol solutions leads to volatilization of HCl, which also partitions with aerosols as a function of pH based on an analogous relationship. These two relationships can be combined and reorganized to yield

$$HCl_g / HNO_{3g} = \left(\left\{Cl^-\right\} / \left\{NO_3^-\right\}\right) * \left[\left(K_{H\text{-}HNO3} * K_{a\text{-}HNO3}\right) / \left(K_{H\text{-}HCl} * K_{a\text{-}HCl}\right)\right] \quad (11)$$

Because the phase partitioning of both species regulates aerosol pH, at equilibrium, the ratio of HCl to HNO_3 in the gas phase is directly proportional to the ratio of Cl^- and NO_3^- activities in aerosol solutions. In addition, aqueous activities for both species covary (and thus mixing ratios of HCl and HNO_3 also covary) as functions of aerosol LWC.

[35] Ranges in aerosol pHs inferred from the measured phase partitioning and associated thermodynamic properties of HCl [*Smith et al.*, 2007] were similar to those estimated during a previous experiment in the same region [*Keene et al.*, 2004]. Briefly, all sampled aerosol size fractions were acidic. Median pH values for the four largest sea-salt size fractions (average GMDs of 25, 13, 6.2, and 2.9 μm) ranged from 3.1 to 3.4 and those for the smallest two size fractions (average GMDs of 0.77 and 0.39 μm) were 1.1 and 1.6, respectively. Total acidity ($H_t = H^+$ + undissociated acids) was greater than H^+ by 1 to 2 orders of magnitude in all size fractions. Most H_t was in the from of HSO_4^- and, consequently, the $HSO_4^- \leftrightarrow H^+ + SO_4^{2-}$ equilibrium substantially buffered aerosol pH. The diel variability in HCl (Figure 5) and HNO_3 [*Fischer et al.*, 2006] implies corresponding variability in aerosol pH [*Keene et al.*, 2004].

[36] In contrast to HCl, HBr is highly soluble in acidic solutions ($K_a = 1.0 \times 10^9$ M; $K_H = 7.2 \times 10^{-1}$ M atm^{-1} (*Chameides and Stelson* [1992] and *Lax* [1969], respectively)) and, consequently, virtually none volatilizes directly from tropospheric aerosols. Model calculations suggest that the production of Br_2 and BrCl in acidified sea-salt solutions (reactions 1 and 2) and their subsequent volatilization are the primary pathways that debrominate marine aerosol [*Sander et al.*, 2003]. Despite the small Br EFs associated with super-μm size fractions, the generally low sea-salt concentrations during this campaign relative to open-ocean conditions and the apparent lack of significant anthropogenic or crustal sources of inorganic Br resulted in relatively low concentrations of volatile inorganic Br. The substantial accumulation of Br in association with sub-μm (primarily pollutant) aerosol size fractions may have also slowed multiphase recycling relative to the open-ocean MBL in which the corresponding Br EFs are substantially lower [*Sander et al.*, 2003]. At these low concentrations, Br-radical chemistry is not expected to significantly influence the chemical evolution of continental outflow in coastal regions.

3.4. Atomic-Cl Production and Steady State Concentration

[37] Model calculations using the approach of *von Glasow and Crutzen* [2004] parameterized for representative conditions during this campaign (S. Pechtl and R. von Glasow, submitted manuscript, 2007) indicate that, at midday, Cl* was composed primarily of HOCl (~60%) and $ClNO_3$ (~36%) with minor additional contributions from ClO, BrCl, and Cl_2 (<~2% each). At midnight, Cl* was composed primarily of $ClNO_2$ (~74%) with the balance contributed by similar amounts of HOCl and Cl_2 (>~13% each). Midday J values for HOCl and $ClNO_2$ were similar but both were about an order of magnitude less that those for Cl_2 (Figure 3h) and about an order of magnitude greater than those for $ClNO_3$ (not shown).

[38] Production rates of atomic Cl were calculated on the basis of three different scenarios (Figure 3i). Scenario1 corresponds to a lower limit for which reaction 5 (HCl + OH) was the only source for atomic Cl. Scenario 2 corresponds to an upper limit that includes the combined production from reaction 5 plus the photolysis of Cl* based on the assumption that Cl* was composed exclusively of Cl_2. Scenario 3 corresponds to a midrange estimate that is identical to scenario 2 except that Cl* was assumed to be composed exclusively of HOCl. It is important to recognize that contributions from Cl* mixing ratios less than the DL were not considered in the analysis but, given the relatively high DL limit (20 pptv Cl), were undoubtedly significant during some periods. Approximate steady state Cl-atom concentrations for each of these scenarios were calculated from equation (9) (Figure 3j).

[39] At HCl mixing ratios greater than about 1 ppbv, reaction with OH typically sustained steady state midday Cl-atom concentrations in the range of 10^4 cm^{-3} (Figure 3); production from photolysis of detectable Cl* contributed to substantially greater Cl-atom concentrations on many days (Figure 3j). These calculations indicate that midday concentrations of atomic Cl in coastal New England during summer often range from 10^4 to 10^5 cm^{-3} and perhaps occasionally higher. The above estimates encompass the average concentrations of atomic Cl (ranging from 2.2 to 5.6 x 10^4 cm^{-3}) that were inferred in parallel on the basis of variability-lifetime relationships for selected NMHCs in surface air associated with the different transport sectors depicted in Figure 2 [*Pszenny et al.*, 2007]. An independent analysis based on relative concentration changes in NMHCs measured during a cruise of the NOAA research vessel *Ronald H. Brown* in the Gulf of Maine during ICARTT yielded similar estimates of Cl-atom concentrations (upper limit of about 4 x 10^4 cm^{-3} [*Goldan et al.*, 2005]). Although the average concentrations inferred from these latter two investigations generally fall within the rather broad range estimated herein (Figure 3j); direct quantitative

evaluation of paired results is constrained by the large uncertainties associated with each approach. For the approach employed in this analysis, the lack of speciation in Cl* and the relatively high DL for Cl* are particularly important in this regard. Despite the inherent limitations, all estimates point to significant concentrations of atomic Cl in polluted continental outflow over the coastal ocean during summer.

[40] Interpretation of paired results for relatively cleaner flow conditions provides useful context for deconvoluting the relative importance of different production pathways. Both *Goldan et al.* [2005] and *Pszenny et al.* [2007] inferred significant Cl-atom concentrations (ranging from 2 to 4 $\times$ 10^4 cm^{-3}) during relatively clean flow conditions associated with multiday transport over the coastal ocean. Although HCl was not measured on the NOAA *Ronald H. Brown* in parallel with the hydrocarbons analyzed by *Goldan et al.* [2005], data from Appledore suggest that the HCl + OH pathway would have been a relatively unimportant source of atomic Cl under these conditions. Appledore experienced persistent relatively clean flow from the "marine" and "south coastal" sectors during two daytime periods (8 and 13 July) for which chemical data are available [e.g., *Fischer et al.*, 2006; *Smith et al.*, 2007]. Although HCl mixing ratios during the late afternoons of most days over the course of the campaign exceeded 1000 pptv (Figure 3e), maximum values for 8 and 13 July were relatively low (360 and 367 pptv, respectively, Figure 3e). These low maxima reflect the efficient loss of anthropogenic acids, particularly HNO_3, and their precursors from aged air parcels over the ocean due to the dry deposition of gases, scavenging and dry deposition via sea salt (e.g., Figure 3b), and wet deposition [*Russell et al.*, 2003; *Fischer et al.*, 2006] and the associated pH-dependent shifts in HCl phase partitioning (see section 3.3). Consequently, under these cleaner conditions, the HCl + OH pathway sustained steady state Cl-atom concentrations during daytime that were also relatively low ($<10^3$ cm^{-3} on 13 July; data for actinic flux were not available for 8 July). In contrast, the corresponding mixing ratios of Cl* were consistently detectable during the afternoons of both days; most exceeded 50 pptv (Figure 3f). Under these conditions, photolysis of Cl* was the major source of atomic Cl, which (on the basis of midrange estimates) sustained steady state concentrations of atomic Cl during the daytime on 13 July of 1.0 to 1.5 $\times$ 10^4 cm^{-3} (Figure 3j). These "midrange" concentrations are reasonably consistent with corresponding estimates based on relative changes in NMHCs and support the hypothesis that direct photolysis of precursors was the dominant production pathway for atomic Cl in aged continental outflow over the coastal ocean. Preliminary model calculations (S. Pechtl and R. von Glasow, submitted manuscript, 2007) indicate that HOCl produced via gas phase recycling (reactions 6 through 8) and Cl_2 produced from reaction of HOCl with Cl^- in acidic aerosol solutions (reaction 3) were the primary Cl-atom precursors in polluted continental outflow over the coastal ocean.

[41] Taken together, results from this and related studies during ICARTT CHAiOS indicate that Cl radicals contributed significantly to the oxidation potential of coastal New England air during summer and thereby modified the chemical processing of continental outflow through the MBL relative to that predicted based exclusively on conventional HO_x/NO_x chemistry. For example, summed reaction rates for methane and more than 30 abundant NMHCs with OH and Cl for air associated with each of the transport sectors suggest that Cl-atom reactions increased the kinetic reactivity of hydrocarbons by 16% to 30% over that due to OH alone [*Pszenny et al.*, 2007]. On the basis of published model calculations [e.g., *Tanaka et al.*, 2003; *Finley and Saltzman*, 2006], we infer that the enhanced supply of odd-H initiated via Cl-hydrocarbon reactions also contributed to net O_3 production. In addition, halogen chemistry would have influenced O_3 production by accelerating the conversion of NO_x to particulate NO_3^- [e.g., *Sander et al.*, 1999] and by altering OH/HO_2 ratios [*Bloss et al.*, 2005]. A companion modeling study (Pechtl and von Glasow, submitted manuscript, 2007) fully evaluates the nature of transformations involving Cl radicals in polluted coastal air and their associated influences on the chemical evolution of continental outflow. Results of that effort are currently in review and will be published separately.

4. Summary and Conclusions

[42] 1. The average concentrations of conservative sea-salt constituents in near-surface air over the coastal Gulf of Maine during summer (e.g., Na^+ = 40 nmol m^{-3}) were factors of 4 to 8 times lower than average values over the open North Atlantic Ocean.

[43] 2. Concentrations of volatile inorganic and particulate Br were at the lower limit of reported values in the MBL. In addition, the inferred production fluxes of sea-salt Cl^- and sea-salt Br^- as functions of transport regime were approximately balanced by the corresponding dry–deposition fluxes of volatile and particulate Cl and Br. These results support the hypothesis that sea-salt aerosol was the primary source for both inorganic Cl and inorganic Br in polluted air along the New England coast.

[44] 3. Acid displacement of sea-salt Cl^- primarily by HNO_3 sustained high HCl mixing ratios (often >2000 pptv) during daytime; based on summed values over all aerosol size fractions, the median Cl^- EF was 0.66. Transport from the more polluted southwest and midwest sectors was associated with relatively lower Cl^- EFs and relatively higher HCl mixing ratios.

[45] 4. Median pH values for the four largest sea-salt size fractions (average GMDs of 25, 13, 6.2, and 2.9 μm) ranged from 3.1 to 3.4 and those for the smallest two size fractions (average GMDs of 0.77 and 0.39 μm) were 1.1 and 1.6, respectively.

[46] 5. Cl* ranged from <20 to 421 pptv but was less than the DL during most sampling intervals. Periods with consistently detectable mixing ratios corresponded to relatively clean conditions, multiday transport over water, and relatively low actinic flux.

[47] 6. At high HCl mixing ratios (>1000 pptv), HCl + OH sustained steady state Cl-atom concentrations in the range of 10^4 cm^{-3}.

[48] 7. Photolysis of detectable Cl* was the dominant source of atomic Cl during many periods; calculated steady state concentrations of Cl atoms were frequently in the range of 10^4 to 10^5 cm^{-3}.

[49] 8. At these concentrations, Cl played an important role in the chemical evolution of the polluted coastal air.

[50] 9. The low production flux of sea-salt aerosol and associated Br^- sustained low concentrations of volatile inorganic and particulate Br compared to the open ocean MBL.

[51] 10. Sub-μm aerosol size fractions were highly enriched in Br; the mechanism(s) responsible for these enrichments are not known.

[52] **Acknowledgments.** We thank two anonymous reviewers for helpful comments. The Shoals Marine Laboratory provided outstanding logistical support, R. Talbot and the AIRMAP Program at the University of New Hampshire (UNH) shared facilities and data, Plymouth State University archived HYSPLIT back trajectories, Andreas Stohl provided FLEXPART retroplumes, and all participants contributed to an intellectually stimulating and thoroughly enjoyable field campaign. Principal financial support was provided by the National Science Foundation (NSF) through awards to the University of Virginia (ATM 0401628), the University of California Los Angeles (UCLA, ATM 0401599), and the University of New Hampshire (UNH, ATM 0401622). Additional support was provided by NOAA through contracts to UNH (NA03OAR4600122, NA04OAR4600154, and NA05OAR4601080) and UCLA (RA133R-04-SE-0411), by the DFG - Emmy Noether Program (grant GL 353-1/1,2), and by NSF through an award to the University of California San Diego (ATM 0401611). This paper is contribution 134 to the Shoals Marine Laboratory.

References

Arimoto, R., R. A. Duce, B. J. Ray, W. G. Ellis Jr., J. D. Cullen, and J. T. Merrill (1995), Trace elements in the atmosphere over the North Atlantic, *J. Geophys. Res.*, *100*, 1199–1213.

Arya, S. P. (2001), *Introduction to Micrometeorology*, 2nd ed., Elsevier, New York.

Atkinson, R. (1997), Gas-phase tropospheric chemistry of volatile organic compounds: 1. Alkanes and alkenes, *J. Phys. Chem. Ref. Data*, *26*, 215–290.

Atkinson, R., D. L. Baulch, R. A. Cox, J. N. Crowley, R. F. Hampson Jr., R. G. Hynes, M. E. Jenkin, J. A. Kerr, M. J. Rossi, and J. Troe (2005), *Summary of Evaluated Kinetic and Photochemical Data for Atmospheric Chemistry*, Subcomm. on Gas Kinet. Data Eval. for Atmos. Chem., Int. Union of Pure and Appl. Chem., Cent. for Atmos. Sci., Univ. of Cambridge, Cambridge, UK. (Available at http://www.iupac-kinetic.ch.cam.ac.uk/)

Bloss, W. J., et al. (2005), Impact of halogen monoxide chemistry upon boundary layer OH and HO_2 concentrations at a coastal site, *Geophys. Res. Lett.*, *32*, L06814, doi:10.1029/2004GL022084.

Chameides, W. L., and A. W. Stelson (1992), Aqueous-phase chemical processes in deliquescent sea-salt aerosols: A mechanism that couples the atmospheric cycles of S and sea salt, *J. Geophys. Res.*, *97*, 20,565–20,580.

DeMore, W., C. Howard, S. Sander, A. Ravishankara, D. Golden, C. Kolb, R. Hampson, M. Molina, and M. Kurylo (1997), Chemical kinetics and photochemical data for use in stratospheric modeling, evaluation 12, *Tech. Rep. JPL 97-4*, Jet Propul. Lab., Calif. Inst. of Technol., Pasadena.

Dickerson, R. R., K. P. Rhoads, T. P. Carsey, S. J. Oltmans, J. P. Burrows, and P. J. Crutzen (1999), Ozone in the remote marine boundary layer: A possible role for halogens, *J. Geophys. Res.*, *104*, 21,385–21,395.

Draxler, R. R., and G. D. Rolph (2005), HYSPLIT (Hybrid Single-Particle Lagrangian Integrated Trajectory) model access via NOAA ARL READY, NOAA Air Resour. Lab., Silver Spring, Md.

Ehhalt, D. H., and F. Rohrer (2000), Dependence of the OH concentration on solar UV, *J. Geophys. Res.*, *105*, 3565–3571.

Erickson, D. J., C. Seuzaret, W. C. Keene, and S.-L. Gong (1999), A general circulation model calculation of HCl and $ClNO_2$ production from sea-salt dechlorination: Reactive Chlorine Emissions Inventory, *J. Geophys. Res.*, *104*, 8347–8372.

Finlayson-Pitts, B. J., M. J. Ezell, and J. N. Pitts (1989), Formation of chemically active chlorine compounds by reactions of atmospheric NaCl particles with gaseous N_2O_5 and $ClONO_2$, *Nature*, *337*, 241–244.

Finlayson-Pitts, B. J., C. J. Koeshian, B. Buehler, and A. S. Ezelle (1999), Kinetics of reaction of chlorine atoms with some biogenic organics, *Int. J. Chem. Kinet.*, *31*, 491–499.

Finley, B., and E. S. Saltzman (2006), Measurement of Cl_2 in coastal urban air, *Geophys. Res. Lett.*, *33*, L11809, doi:10.1029/2006GL025799.

Fischer, E., A. Pszenny, W. Keene, J. Maben, A. Smith, A. Stohl, and R. Talbot (2006), Nitric acid phase partitioning and cycling in the New England coastal atmosphere, *J. Geophys. Res.*, *111*, D23S09, doi:10.1029/2006JD007328.

Galbally, I. E., S. T. Bentley, and C. P. Meyer (2000), Mid-latitude marine boundary-layer ozone destruction at visible sunrise observed at Cape Grim, Tasmania, *Geophys. Res. Lett.*, *27*, 3841–3844.

Galloway, J. N., D. L. Savoie, W. C. Keene, and J. M. Prospero (1993), The temporal and spatial variability of scavenging ratios for nss sulfate, nitrate, methanesulfonate and sodium in the atmosphere over the North Atlantic Ocean, *Atmos. Environ., Part A*, *27*, 235–250.

Goldan, P. D., W. C. Kuster, M. Shao, and F. C. Fehsenfeld (2005), Hydrocarbon measurements aboard the Ron Brown during NEAQS 2004: Chemical time scales and evidence of chlorine chemistry in the marine boundary layer, *Eos Trans. AGU*, *86*(52), Fall Meeting Suppl., Abstract A21A-0829.

Graedel, T. E., and W. C. Keene (1995), The tropospheric budget of reactive chlorine, *Global Biogeochem. Cycles*, *9*, 47–78.

Honninger, G., C. von Friedeburg, and U. Platt (2004), Multi axis differential optical absorption spectroscopy (MAX-DOAS), *Atmos. Chem. Phys.*, *4*, 231–254.

Hummelshøj, P., N. O. Jensen, and S. E. Larsen (1992), Particle dry deposition to a sea surface, in *Precipitation Scavenging and Atmosphere-Surface Exchange*, edited by S. E. Schwartz and W. G. N. Slinn, pp. 829–841, Taylor and Francis, Philadelphia, Pa.

Keene, W. C., and D. L. Savoie (1998), The pH of deliquesced sea-salt aerosol in polluted marine air, *Geophys. Res. Lett.*, *25*, 2181–2194, (Correction, *Geophys. Res. Lett.*, *26*, 1315–1316, 1999).

Keene, W. C., A. A. P. Pszenny, J. N. Galloway, and M. E. Hawley (1986), Sea-salt corrections and interpretation of constituent ratios in marine precipitation, *J. Geophys. Res.*, *91*, 6647–6658.

Keene, W. C., et al. (1989), An intercomparison of measurement systems for vapor- and particulate-phase concentrations of formic and acetic acids, *J. Geophys. Res.*, *94*, 6457–6471.

Keene, W. C., A. A. P. Pszenny, D. J. Jacob, R. A. Duce, J. N. Galloway, J. J. Schultz-Tokos, H. Sievering, and J. F. Boatman (1990), The geochemical cycling of reactive chlorine through the marine troposphere, *Global Biogeochem. Cycles*, *4*, 407–430.

Keene, W. C., J. R. Maben, A. A. P. Pszenny, and J. N. Galloway (1993), Measurement technique for inorganic chlorine gases in the marine boundary layer, *Environ. Sci. Technol.*, *27*, 866–874.

Keene, W. C., R. Sander, A. A. P. Pszenny, R. Vogt, P. J. Crutzen, and J. N. Galloway (1998), Aerosol pH in the marine boundary layer: A review and model evaluation, *J. Aerosol Sci.*, *29*, 339–356.

Keene, W. C., et al. (1999), Composite global emissions of reactive chlorine from natural and anthropogenic sources: Reactive Chlorine Emissions Inventory, *J. Geophys. Res.*, *104*, 8429–8440.

Keene, W. C., A. A. P. Pszenny, J. R. Maben, E. Stevenson, and A. Wall (2004), Closure evaluation of size-resolved aerosol pH in the New England coastal atmosphere during summer, *J. Geophys. Res.*, *109*, D23307, doi:10.1029/2004JD004801.

Keene, W. C., J. M. Lobert, P. J. Crutzen, J. R. Maben, D. H. Scharffe, T. Landmann, C. Hély, and C. Brain (2006), Emissions of major gaseous and particulate species during experimental burns of southern African biomass, *J. Geophys. Res.*, *111*, D04301, doi:10.1029/2005JD006319.

Lax, E. (1969), *Taschenbuch für Chemiker und Physiker*, Springer, New York.

Lewis, E. R., and S. E. Schwartz (2004), *Sea Salt Aerosol Production: Mechanisms, Methods, Measurements, and Models: A Critical Review*, *Geophys. Monogr. Ser.*, vol. 152, AGU, Washington, D. C.

Li, S. M., Y. Yokouchi, L. A. Barrie, K. Muthuramu, P. B. Shepson, J. W. Bottenheim, W. T. Sturges, and S. Landsberger (1994), Organic and inorganic bromine compounds and their composition in the Arctic troposphere during polar sunrise, *J. Geophys. Res.*, *99*, 25,415–25,428.

Maben, J. R., W. C. Keene, A. A. P. Pszenny, and J. N. Galloway (1995), Volatile inorganic chlorine in surface air over eastern North America, *Geophys. Res. Lett.*, *22*, 3513–3516.

Martinez, M., T. Arnold, and D. Perner (1999), The role of bromine and chlorine chemistry for arctic ozone depletion events in Ny-Ålesund and comparison with model calculations, *Ann. Geophys.*, *17*, 941–956.

Nagao, I., K. Matsumoto, and H. Tanaka (1999), Sunrise ozone destruction found in the sub-tropical marine boundary layer, *Geophys. Res. Lett.*, *26*, 3377–3380.

Pikelnaya, O., S. C. Hurlock, S. Trick, and J. Stutz (2007), Intercomparison of multi-axis and long-path DOAS measurements in the marine boundary layer, *J. Geophys. Res.*, doi:10.1029/2006JD007727, in press.

Pszenny, A. A. P., W. C. Keene, D. J. Jacob, S. Fan, J. R. Maben, M. P. Zetwo, M. Springer-Young, and J. N. Galloway (1993), Evidence of inorganic chlorine gases other than hydrogen chloride in marine surface air, *Geophys. Res. Lett.*, *20*, 699–702.

Pszenny, A. A. P., J. Moldanová, W. C. Keene, R. Sander, J. R. Maben, M. Martinez, P. J. Crutzen, D. Perner, and R. G. Prinn (2004), Halogen

cycling and aerosol pH in the Hawaiian marine boundary layer, *Atmos. Chem. Phys.*, *4*, 147–168.

Pszenny, A. A. P., E. V. Fischer, R. S. Russo, B. C. Sive, R. K. Varner, and A. White (2007), Estimates of Cl atom concentrations and hydrocarbon kinetic reactivity in surface air at Appledore Island, Maine (USA) during ICARTT CHAiOS, *J. Geophys. Res.*, doi:10.1029/2006JD007725, in press.

Rancher, J., and M. A. Kritz (1980), Diurnal fluctuation of Br and I in the marine atmosphere, *J. Geophys. Res.*, *85*, 5581–5587.

Russell, K. M., W. C. Keene, J. R. Maben, J. N. Galloway, and J. L. Moody (2003), Phase partitioning and dry deposition of atmospheric nitrogen at the mid-Atlantic U. S. coast, *J. Geophys. Res.*, *108*(D21), 4656, doi:10.1029/2003JD003736.

Russell, L. M., A. A. Mensah, E. V. Fisher, B. C. Sive, R. K. Varner, W. C. Keene, J. Stutz, and A. A. P. Pszenny (2007), Nanoparticle growth Following photochemical α- and β- pinene oxidation at Appledore Island during ICARTT/CHAiOS 2004, *J. Geophys. Res.*, doi:10.1029/2006JD007736, in press.

Sander, R., Y. Rudich, R. von Glasow, and P. J. Crutzen (1999), The role of $BrNO_3$ in marine tropospheric chemistry: A model study, *Geophys. Res. Lett.*, *26*, 2858–2860.

Sander, R., et al. (2003), Inorganic bromine in the marine boundary layer: A critical review, *Atmos. Chem. Phys.*, *3*, 1301–1336. (Available at http://www.atmos-chem-phys.org/acp/3/1301).

Singh, H. B., and J. F. Kasting (1988), Chlorine-hydrocarbon photochemistry in the marine troposphere and lower stratosphere, *J. Atmos. Chem.*, *7*, 261–285.

Sive, B. C., D. D. Shively, and B. M. C. Pape (2003), Spatial variation and characteristics of volatile organic compounds associated with snowmobile emissions in Yellowstone National Park, report, Off. of Plann. and Compliance, Natl. Park Serv., U.S. Dep. of the Inter., Washington, D. C. (Available at http://www.nps.gov/yell/technical/planning/winteruse/plan/sive_report.htm)

Sive, B. C., Y. Zhou, D. Troop, Y. Li, W. Little, O. W. Wingenter, R. S. Russo, R. K. Varner, and R. W. Talbot (2005), Development of a cryogen-free concentration system for measurements of volatile organic compounds, *Anal. Chem.*, *77*, 6989–6998, doi:10.1021/ac0506231.

Smith, A. M., W. C. Keene, J. R. Maben, A. A. P. Pszenny, E. Fischer, and A. Stohl (2007), Ammonia sources, transport, transformation, and deposition in coastal New England during summer, *J. Geophys. Res.*, doi:10.1029/2006JD007574, in press.

Spicer, C. W., E. G. Chapman, B. J. Finlayson-Pitts, R. A. Plastridge, J. M. Hubbe, J. D. Fast, and C. M. Berkowitz (1998), Observations of molecular chlorine in coastal air, *Nature*, *394*, 355–356.

Stohl, A., C. Forster, A. Frank, P. Seibert, and G. Wotawa (2005), Technical note: The Lagrangian particle dispersion model FLEXPART version 6.2, *Atmos. Chem. Phys.*, *5*, 2461–2474.

Stutz, J., R. Ackermann, J. D. Fast, and L. Barrie (2002), Atmospheric reactive chlorine and bromine at the Great Salt Lake, Utah, *Geophys. Res. Lett.*, *29*(10), 1380, doi:10.1029/2002GL014812.

Tanaka, P. L., et al. (2003), Direct evidence for chlorine-enhanced urban ozone formation in Houston, Texas, *Atmos. Environ.*, *37*, 1393–1400.

Valigura, R. A. (1995), Iterative bulk exchange model for estimating air-water transfer of HNO_3, *J. Geophys. Res.*, *100*(D12), 26,045–26,050.

Vogt, R., P. J. Crutzen, and R. Sander (1996), A mechanism for halogen release from sea-salt aerosol in the remote marine boundary layer, *Nature*, *383*, 327–330.

von Glasow, R., and P. J. Crutzen (2004), Model study of multiphase DMS oxidation with a focus on halogens, *Atmos. Chem. Phys.*, *4*, 589–608.

von Glasow, R., R. Sander, A. Bott, and P. J. Crutzen (2002), Modeling halogen chemistry in the marine boundary layer: 2. Interactions with sulfur and the cloud-covered MBL, *J. Geophys. Res.*, *107*(D17), 4323, doi:10.1029/2001JD000943.

Willeke, K. (1975), Performance of the slotted impactor, *Am. Ind. Hygiene Assoc. J.*, *36*, 683–691.

Wilson, T. R. S. (1975), Salinity and the major elements of sea water, in *Chemical Oceanography*, vol. 1, 2nd ed., edited by J. P. Riley, and G. Skirrow, pp. 365–413, Elsevier, New York.

Zhou, Y. (2006), Atmospheric volatile organic compound measurements: Distributions and effects on air quality in coastal marine, rural and remote continental environments, Ph.D.Dissertation, Univ. of N. H., Durham.

Zhou, Y., R. K. Varner, R. S. Russo, O. W. Wingenter, K. B. Haase, R. Talbot, and B. C. Sive (2005), Coastal water source of short-lived halocarbons in New England, *J. Geophys. Res.*, *110*, D21302, doi:10.1029/2004JD005603.

E. V. Fischer, Department of Atmospheric Sciences, University of Washington, Seattle, WA 98195, USA.

W. C. Keene and J. R. Maben, Department of Environmental Sciences, University of Virginia, Charlottesville, VA 22904, USA. (wck@virginia.edu)

S. Pechtl, Deutsches Patent- und Markenamt, Munich, D-80331, Germany.

A. A. P. Pszenny, B. C. Sive, and R. K. Varner, Institute for the Study of Earth, Oceans, and Space, University of New Hampshire, Durham, NH 03824, USA.

A. M. Smith, Pollard Environmental, LLC, Richmond, VA 23233, USA.

J. Stutz, Department of Atmospheric and Oceanic Sciences, University of California, Los Angeles, CA 90095, USA.

R. von Glasow, School of Environmental Sciences, University of East Anglia, Norwich, NR4 7TJ, UK.